Neuronal cytoskeletal gene dysregulation and mechanical hypersensitivity in a rat model of Rett syndrome

Aritra Bhattacherjee[a,b], Ying Mu[a], Michelle K. Winter[b], Jennifer R. Knapp[b], Linda S. Eggimann[b], Sumedha S. Gunewardena[a,b], Kazuto Kobayashi[c], Shigeki Kato[c], Dora Krizsan-Agbas[a], and Peter G. Smith[a,b,1]

[a]Department of Molecular and Integrative Physiology, University of Kansas Medical Center, Kansas City, KS 66160; [b]Kansas Intellectual and Developmental Disabilities Research Center, University of Kansas Medical Center, Kansas City, KS 66160; and [c]Department of Molecular Genetics, Institute of Biomedical Sciences, Fukushima Medical University School of Medicine, Fukushima 9601295, Japan

Edited by Michael E. Greenberg, Harvard Medical School, Boston, MA, and approved July 6, 2017 (received for review November 7, 2016)

Children with Rett syndrome show abnormal cutaneous sensitivity. The precise nature of sensory abnormalities and underlying molecular mechanisms remain largely unknown. Rats with methyl-CpG binding protein 2 (MeCP2) mutation, characteristic of Rett syndrome, show hypersensitivity to pressure and cold, but hyposensitivity to heat. They also show cutaneous hyperinnervation by nonpeptidergic sensory axons, which include subpopulations encoding noxious mechanical and cold stimuli, whereas peptidergic thermosensory innervation is reduced. MeCP2 knockdown confined to dorsal root ganglion sensory neurons replicated this phenotype in vivo, and cultured MeCP2-deficient ganglion neurons showed augmented axonogenesis. Transcriptome analysis revealed dysregulation of genes associated with cytoskeletal dynamics, particularly those controlling actin polymerization and focal-adhesion formation necessary for axon growth and mechanosensory transduction. Down-regulation of these genes by topoisomerase inhibition prevented abnormal axon sprouting. We identified eight key affected genes controlling actin signaling and adhesion formation, including members of the Arhgap, Tiam, and cadherin families. Simultaneous virally mediated knockdown of these genes in Rett rats prevented sensory hyperinnervation and reversed mechanical hypersensitivity, indicating a causal role in abnormal outgrowth and sensitivity. Thus, MeCP2 regulates ganglion neuronal genes controlling cytoskeletal dynamics, which in turn determines axon outgrowth and mechanosensory function and may contribute to altered pain sensitivity in Rett syndrome.

autism | axon growth | dorsal root ganglion | pain

Rett syndrome (OMIM No. 312750: RTT) is a severe autism-associated pervasive developmental disorder afflicting 1 in 10,000 live female births with progressive psychomotor, verbal, and intellectual impairments (1, 2). Mutation of the X-linked gene, methyl-CpG binding protein 2 (*MECP2*), was identified as a principal underlying cause of RTT (3, 4). MeCP2 protein is crucial for brain development, as evidenced by abnormal neuronal morphology in MeCP2 KO mice (5–7), consistent with cognitive impairment (8). Hence, altered CNS structure and function secondary to MeCP2 mutation are accepted as probable substrates for intellectual, motor, and social disabilities associated with RTT.

Patients with RTT appear to show somatosensory disturbances, including abnormal response to touch. Caregivers often report behaviors consistent with insensitivity, or elevated pain threshold, in RTT patients (9–11). However, these studies are inherently confounded by the nonverbal nature of the disorder and the severe motor impairment (12, 13). Subsequent reports conclude that substantial proportions of the RTT population frequently display pain-associated behaviors, which may be modality-specific (12–15). Therefore, although the literature supports the idea that sensory function is disturbed in RTT, the nature and extent to which nociceptor function are affected remain unclear.

There is reason to suggest that changes in peripheral sensory neurons underlie sensory dysfunction in RTT and related developmental disorders. Individuals with pervasive developmental disorders, including RTT, often exhibit self-injurious behavior and skin biopsies reveal sensory hyperinnervation (16, 17), implying abnormal regulation of peripheral axon growth. Moreover, abnormal tactile sensitivity has been observed in a mouse model of RTT, and MeCP2 mutation confined to peripheral neurons can replicate this phenotype (18). However, the extent to which MeCP2 mutation affects the peripheral sensory neuron transcriptome and axonal outgrowth are unknown.

We present evidence that MeCP2 plays a major role in regulating peripheral sensory innervation and determining mechanical and thermal behavioral sensitivity. Our findings in the RTT rat show modality-specific behavioral effects, altered dorsal root ganglion (DRG) axon outgrowth, and transcriptional changes in cytoskeleton-associated genes obligatory to axon growth and mechanical transduction.

Results

RTT Rats Show Abnormal Mechanical and Temperature Sensitivity. We sought to determine if mechanical or thermal sensitivity is altered in an animal model of RTT. The rat is the preferred model for assessing sensory behavior (19), and we used Sprague-Dawley rats harboring a RTT-like mutation consisting of a 71-bp (53,900 to 53,970-bp) zinc finger nuclease-mediated deletion in exon 4 of *Mecp2* (#TGRA6090; SAGE Labs). All studies were

Significance

Cutaneous sensitivity appears to be abnormal in Rett syndrome and other autistic disorders. Using rats with disrupted methyl-CpG binding protein 2 (MeCP2) expression characteristic of Rett syndrome, we found that MeCP2 deficiency in sensory neurons led to augmented pressure and cold sensitivity but hyposensitivity to heat, accompanied by respective changes in cutaneous innervation. Transcriptome analysis of MeCP2-deficient ganglia showed up-regulation of genes associated with actin cytoskeletal dynamics and adhesion formation; down-regulating key genes in vivo normalized both mechanical sensitivity and innervation density. These findings provide evidence that ganglion cytoskeletal genes play key roles in determining mechanosensory properties, which may contribute to altered pain sensitivity in Rett syndrome and other painful conditions.

Author contributions: A.B. and P.G.S. designed research; A.B., Y.M., M.K.W., L.S.E., and D.K.-A. performed research; K.K. and S.K. contributed new reagents/analytic tools; A.B., Y.M., M.K.W., J.R.K., S.S.G., and P.G.S. analyzed data; and A.B. and P.G.S. wrote the paper.

The authors declare no conflict of interest.

This article is a PNAS Direct Submission.

Data deposition: The data reported in this paper have been deposited in the Gene Expression Omnibus (GEO) database, https://www.ncbi.nlm.nih.gov/geo (accession no. GSE87855).

[1]To whom correspondence should be addressed. Email: psmith@kumc.edu.

This article contains supporting information online at www.pnas.org/lookup/suppl/doi:10.1073/pnas.1618210114/-/DCSupplemental.

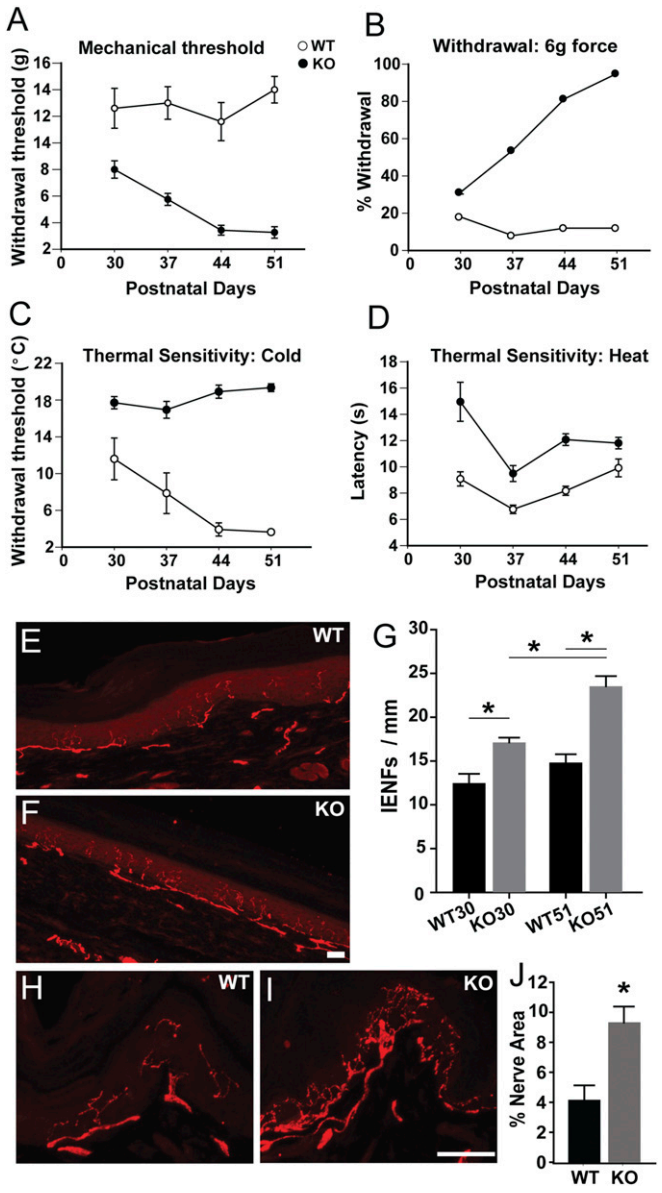

Fig. 1. Sensory behavior and peripheral innervation are altered in MeCP2 KO rats. (*A*) Mechanical threshold (force in *g*) measured weekly between 30 and 51 d. Responses of the *Mecp2*$^{-/y}$ (KO) rat were lower at all ages compared with WT rat ($P < 0.001$), becoming more pronounced at later ages ($P < 0.001$ genotype × strain interaction). WT showed increased threshold with age ($P < 0.005$ for 51 d vs. 30 and 37 d). (*B*) Mechanical sensitivity assessed as percent withdrawal to a normally subthreshold (6 *g*) stimulus. Responses of the KO rat were greater at all ages ($P < 0.001$), and became more pronounced at later ages ($P < 0.001$ genotype × strain interaction). WT response frequency remained constant, whereas KO responses were greater than 30 d at all other ages ($P \leq 0.005$). (*C*) Cold plate temperature inducing a withdrawal response. The KO rat showed lower cold tolerance at all ages ($P < 0.001$) and remained constant throughout the testing period, whereas WT rats were more sensitive at 44 and 51 d relative to 30 d ($P \leq 0.01$). (*D*) Noxious heat sensitivity defined as latency in seconds before a withdrawal response. KO rats were less sensitive to heat at all ages ($P < 0.001$). In *A–D*, significance was assessed by two-way repeated-measure ANOVA with post hoc comparisons using the Holm–Sidak method (n = 5 WT, 6 KO). (*E*) Immunostaining for PGP9.5 in footpad section of WT rat showing IENFs. (*F*) PGP9.5-ir IENFs in footpad section of KO rat. (Scale bar, 50 μm.) (*G*) IENF per unit length of the epidermis is greater in KO than in WT animals at both 30 and 51 d, with KO innervation increasing in this period. *P = 0.014 WT30 vs. KO30; $P < 0.001$, WT51 vs. KO51; $P = 0.001$, KO30 vs. KO51; $P = 0.0153$, WT30 vs. WT51. n at 30 d = 4 WT, 5 KO; n at 51 d = 8 WT, 9 KO. (*H*) PGP9.5 immunostaining in dorsal hairy skin epithelium in WT rat. (*I*) PGP9.5-ir in dorsal hairy skin epithelium of KO rat. (Scale bar, 50 μm.) (*J*) Quantitative comparison of PGP9.5-ir innervation density in dorsal hairy skin of WT and KO rats at 51 d (*P = 0.02; n = 5 WT, 6 KO).

conducted in male KO rats (*Mecp2*$^{-/y}$), as their phenotype is severe and more closely resembles the human form of RTT, and age-matched male Sprague-Dawley WT (*Mecp2*$^{x/y}$) rats. To determine if MeCP2 KO rats show altered nocifensive behaviors, we used standard sensorimotor behavioral tests in MeCP2 KO and WT control rats. The behavioral phenotype of the MeCP2 KO rat has been characterized previously (20–22) and is similar to that of mouse models (8). Our rats showed lower axon outgrowth from CNS neurons, and reduced ambulatory activity and motor performance at 30–51 d (Fig. S1) that was not so severe as to impair sensory testing.

Commencing at 30 d, hind paw sensitivity to touch, noxious heat, and cold were measured weekly for 3 wk. Mechanical sensitivity was assessed by von Frey analgesiometry, which measures force needed to elicit hind paw withdrawal (mechanical threshold). We also determined how frequently a stimulus that is below threshold for most control subjects (6 g) elicited a response. Control rats showed stable mechanical withdrawal thresholds throughout the testing period (Fig. 1*A*). MeCP2 KO rats displayed lower thresholds at 30 d, and became increasingly sensitive through 51 d. Similarly, responses to the subthreshold stimulus occurred more often and increased with age in MeCP2 KO rats (Fig. 1*B*).

Cold sensitivity was measured using a cold plate with a declining temperature of 10 °C/min. MeCP2 KO rats responded aversively to smaller declines, indicating increased cold sensitivity at all ages (Fig. 1*C*). Noxious heat sensitivity was measured according to the Hargreaves plantar analgesia method, with sensitivity defined as latency in responding to footpad warming. WT rats showed little change with age. In contrast, KO animals showed longer latencies, indicating reduced sensitivity (Fig. 1*D*).

Cutaneous Targets Are Hyperinnervated in RTT Rats. We posited that behavioral anomalies seen in *Mecp2*$^{-/y}$ rats may be associated with altered innervation patterns. We examined glabrous skin of the hind paw in regions corresponding to those used for sensory testing in rats at 30 and 51 d. In control rats, immunostaining for the panneuronal marker PGP9.5 revealed axons coursing beneath and parallel to the epidermis, sending intraepidermal nerve fibers (IENFs) toward the surface (Fig. 1*E*). In KO rats, subepithelial and epithelial innervation appeared more abundant (Fig. 1*F*) and quantitative analysis showed greater numbers of IENFs per unit length of glabrous skin, becoming more pronounced with age (Fig. 1*G*). We queried whether increased innervation is restricted to glabrous skin or occurs elsewhere. Examination of dorsal hairy skin epithelium revealed complex axon geometry in control rats (Fig. 1*H*), and numbers of PGP9.5-immunoreactive (-ir) fibers were strikingly more abundant in KO rats (Fig. 1 *I* and *J*). These observations suggest that MeCP2 regulates DRG axonal outgrowth in neurons innervating multiple peripheral targets.

Sensory Axon Subpopulations Are Affected Differentially in RTT Rats. MeCP2 is expressed widely in neurons (23, 24), including those in DRGs (25, 26), where it binds methylated cytosine in DNA, thereby regulating gene expression (27). We confirmed that all DRG neurons strongly express nuclear MeCP2 (Fig. S2 *A* and *B*) at levels comparable to CNS neurons (Fig. S2 *C* and *D*). Expression was prominent in neurons positive for the peptidergic neuronal marker calcitonin gene-related peptide (CGRP) (Fig. S2 *E–H*), the nonpeptidergic neuronal marker isolectin B4 (IB4) (Fig. S2 *I–L*), and large diameter myelinated neuronal marker neurofilament H (NFH) (Fig. S2 *M–P*).

Because thermal and mechanical sensory modalities are altered differently by MeCP2 disruption, we wondered if this might reflect selective differences in subpopulations of cutaneous

axons. Footpad sections from rats were costained for PGP9.5 and CGRP to identify sensory axons responsive to noxious heat (28), and distinguish them from nonpeptidergic mechanosensitive axons (29). In WT rats, PGP9.5-ir fibers often display CGRP-ir (Fig. 2 *A–C*). In KO rats, PGP9.5-ir IENFs were encountered more frequently but fewer fibers appeared to be costained with CGRP (Fig. 2 *D–F*), suggesting that hyperinnervation is primarily a result of proliferation of nonpeptidergic fibers. To assess relative distributions, we counted PGP9.5-ir fibers that were either $CGRP^+$ (peptidergic) or $CGRP^-$ (nonpeptidergic) in samples at 30 and 51 d. Quantitation indicated that numbers of nonpeptidergic fibers were increased in KO (Fig. 2*G*), whereas peptidergic axons were reduced at both 30 and 51 d (Fig. 2*H*). NFH-ir axons were restricted to the lower dermis, and therefore did not contribute to IENFs. Subepidermal areas occupied by NFH-ir axons was modestly increased in MeCP2 KO rats (0.54 ± 0.03% in WT, 0.65 ± 0.03% in KO, $P = 0.04$).

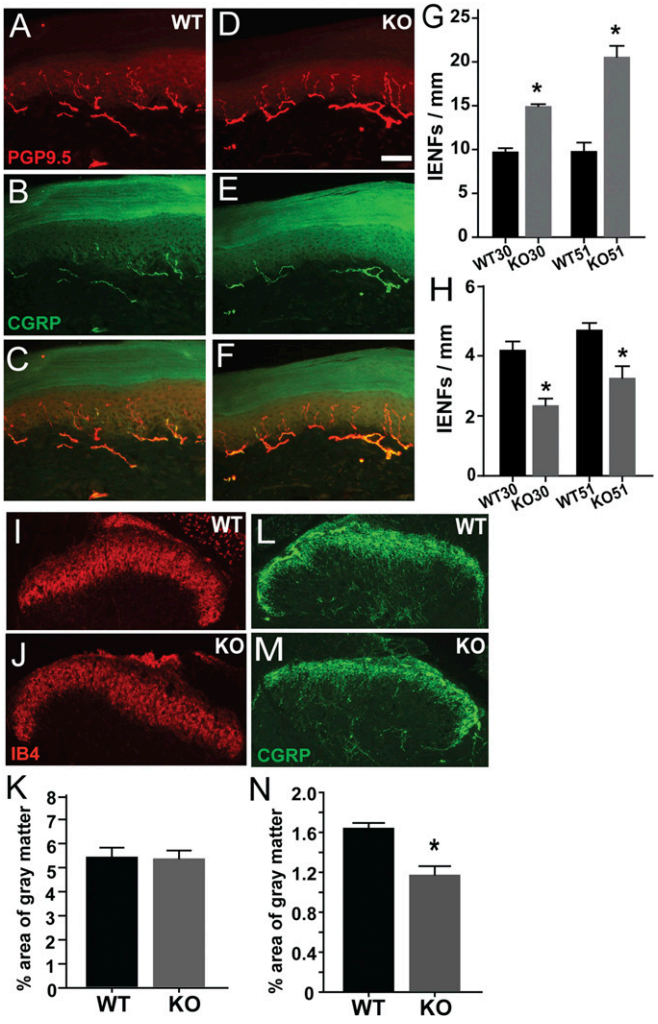

Fig. 2. MeCP2 KO affects peptidergic and nonpeptidergic sensory axons differentially in vivo. (*A–H*) Footpad innervation. WT rat footpad section immunostained for PGP9.5 (*A*) and CGRP (*B* and *C*), and *Mecp2*$^{-/y}$ (KO) rat section stained for PGP9.5 (*D*) and CGRP (*E* and *F*) at 51 d. Quantitative analyses show nonpeptidergic innervation ($PGP9.5^+$, $CGRP^-$) is increased in KO skin at 30 and 51 d (*G*: *$P = 0.01$, WT30 vs. KO30; $P = 0.001$, WT51 vs. KO51; $P = 0.001$, KO30 vs. KO51 = 0.001). CGRP-ir peptidergic innervation is reduced (*H*: *$P = 0.003$, WT30 vs. KO30; $P < 0.001$, WT51 vs. KO51; $P = 0.05$, KO30 vs. KO51; 30 d, $n = 4$ WT, 5 KO; 51 d, $n = 8$ WT, 9 KO) (*I–N*) Spinal cord innervation. IB4 staining of the spinal dorsal horn reveals nonpeptidergic innervation in wild type and KO rats (*I* and *J*), which is comparable in both genotypes (*K*). CGRP immunostaining identifies peptidergic fibers (*L* and *M*), and quantitation shows that these are reduced in the KO rat (*N*, *$P = 0.003$, $n = 5$ WT, 6 KO). (Scale bar in *D*, 50 μm; applies to all micrographs.)

We next examined the spinal cord to determine if DRG central projections are affected by MeCP2 disruption. Dorsal horns of WT rats showed robust IB4-labeled innervation that was unchanged in KO rats (Fig. 2 *I–K*). However, density of CGRP terminals was reduced relative to WT (Fig. 2 *L–N*). Hence, MeCP2 mutation is associated with increased nonpeptidergic innervation in peripheral cutaneous targets, whereas both central and peripheral peptidergic innervation is reduced.

MeCP2 Dysregulation in DRG Neurons Increases Neurite Outgrowth in Vitro. We next addressed whether MeCP2 dysfunction in DRG neurons is the direct cause of altered sensory nerve density in MeCP2 KO rats. Previous studies have implicated MeCP2 downregulation in axon outgrowth (25), suggesting that MeCP2 may normally suppress neuritogenesis. We confirmed that DRGs from KO rats showed absence of detectable MeCP2 protein (Fig. 3*A*). Dissociated DRG neurons from 30- to 35-d KO and WT rats were cultured for 48 h. Control neurite outgrowth was similar to that seen previously (30), whereas KO outgrowth was 44% greater (Fig. 3 *B–D*). Small-diameter unmyelinated DRG neurons were identified in culture by expression of peripherin (31). Peripherin-ir neurons with CGRP-ir were evident, and neurite outgrowth was increased by 38% in KO relative to WT (Fig. 3 *E–G*). Peripherin-ir neurons lacking CGRP were also present in both strains, and these nonpeptidergic neurons showed 39% greater outgrowth in KO cultures (Fig. 3 *H–J*). Large-diameter myelinated neurons expressing NFH extended longer axons and axon outgrowth was increased by 22% in KO cultures (Fig. 3 *K–M*). Thus, loss of MeCP2 function up-regulates intrinsic neurite growth potential in multiple DRG neuronal subpopulations in vitro.

MeCP2 Knockdown in DRG Neurons Produces Hyperinnervation and Hypersensitivity in WT Rats. Although in vitro studies show that MeCP2 KO directly increases DRG axonal outgrowth, it is unclear whether altered sensitivity in the KO rat is because of effects on the primary afferent neuron or higher-order systems. We therefore assessed the impact of MeCP2 dysfunction confined to DRG by selective knockdown of MeCP2 in neurons innervating the hind paw of WT rats.

We first confirmed knockdown efficiency of shRNA in the rat 50B11 sensory neuronal cell line (32, 33). Selected shRNAs that reduced MeCP2 protein by >80% (Fig. 4*A*) were then cloned to an EGFP-expressing vector backbone and used for lentiviral transduction of dissociated DRG neurons from 30- to 35-d rats. Lentiviral particles were engineered to include rabies virus coat protein sequences in the FuGB2 envelope plasmid, which increases retrograde transport efficiency (34). Transduced WT neurons showed strong EGFP but lacked nuclear MeCP2-ir (Fig. 4 *B–D*). Neurons transduced with scrambled shRNA at 48 h showed neurite outgrowth typical of WT neurons (Fig. 4*E*). Transduction with MeCP2 shRNA induced profuse neurite outgrowth, increasing overall length ~twofold (Fig. 4 *F* and *G*), confirming MeCP2's role in normally suppressing axon outgrowth.

We achieved stable neuronal transduction of DRG neurons in vivo by injecting hind paws of 6- to 7-d rats with the FuGB2 lentiviral shRNA, whereas contralateral paws were injected with virus particles containing scrambled shRNA. Thirty days following injection, hind paws were tested for mechanical and thermal sensitivity, and epidermis and L4–L6 DRGs removed for analysis. DRG sections showed numerous GFP-ir neurons (Fig. 4*H*). Transduction efficiency of both peptidergic and nonpeptidergic neurons was comparable (Fig. S3), and hind paw skin contained appreciable subepidermal and epidermal GFP-ir fibers (Fig. 4 *I* and *J*).

We assessed whether selective peripheral MeCP2 knockdown affects hind paw innervation density. Paws receiving scrambled shRNA lentivirus showed cutaneous PGP9.5-ir innervation patterns that were essentially indistinguishable from uninjected foot

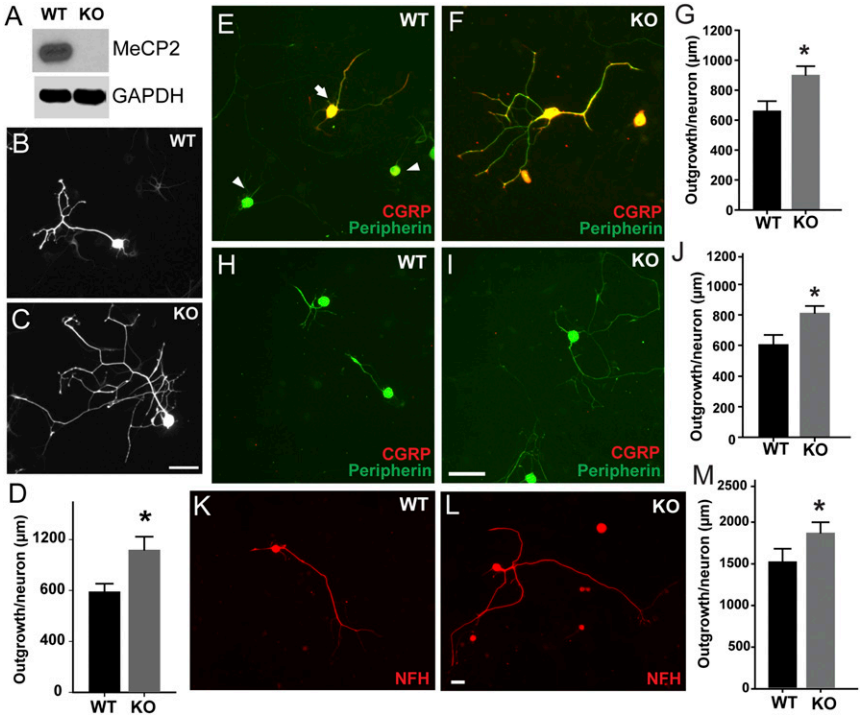

Fig. 3. MeCP2 regulates sensory neurite outgrowth in vitro. (*A*) DRG lysates from *Mecp2*$^{-/y}$ KO animals show MeCP2 protein ablation. (*B–D*) MeCP2 KO neurons show increased neurite outgrowth (*P = 0.01, n = 50–75 neurons per group). Cultured DRG neurons from WT (*E*) and KO (*F*) rats costained for peripherin and CGRP show peptidergic (arrow) and nonpeptidergic (arrowhead) neurons. (*G*) Quantitation shows increased neurite outgrowth by peptidergic KO neurons (*P = 0.007, n = 50–75 neurons per group). (*H*) Peripherin-ir neurons lacking CGRP-ir were identified in WT rats. (*I*) Peripherin^{+}, CGRP^{-} neurons were also present in KO rats, and appeared to have more complex neurite geometries. (*J*) Quantitative analysis shows increased total neurite outgrowth per neuron in KO rats (*P = 0.027, n = 50–75 neurons per group). (*K*) NFH is a marker of larger myelinated DRG neurons, and staining for this protein revealed many neurons in WT cultures. (*L*) Cultures from KO rats also contained NFH-ir neurons. (*M*) Total neurite length was increased in KO neurons (*P = 0.041, n = 50–75 neurons per group). (Scale bars, 50 μm.)

pads (Fig. 4*K*). In contrast, MeCP2 knockdown paws had greater numbers of sub- and intraepithelial nerve fibers (Fig. 4 *L* and *M*). Footpads receiving scrambled shRNA displayed CGRP-ir innervation that was similar to uninjected controls (Fig. 4*N*), and this was not affected by MeCP2 knockdown (Fig. 4 *O* and *P*), indicating that the increased PGP9.5-ir innervation density is a result of nonpeptidergic fiber proliferation. Image analysis of lumbar spinal cord sections did not show detectable changes in either IB4^{+} or CGRP^{+} innervation (Fig. S4).

To determine whether differences in peripheral innervation are accompanied by behavioral changes, we assessed mechanical and heat sensitivity (the single-paw injection strategy was not compatible with cold testing). Relative to rats receiving control shRNA, those transduced with MeCP2 knockdown shRNA showed withdrawal responses at lower force (Fig. 4*Q*) and responded more frequently to subthreshold stimuli (Fig. 4*R*). In contrast, response latency to noxious heat did not differ relative to controls (Fig. 4*S*). MeCP2 dysregulation restricted to peripheral sensory DRG neurons is therefore sufficient to elicit increased sensitivity to mechanical (but not thermal) stimuli in conjunction with increased nonpeptidergic innervation density.

MeCP2 Disruption Selectively Regulates DRG Functional Pathways. Because MeCP2 down-regulation in peripheral neurons essentially replicates the phenotype seen in the RTT rat model, we focused on transcriptional changes within the DRG to better understand underlying mechanisms. We performed whole-transcriptome sequencing of RNA isolated from KO and WT DRGs (GEO accession no. GSE87855). A heat map plot revealed clustering by genotypic variation and differential expression of a wide range of genes (Fig. 5*A* and Fig. S5). Several previously identified CNS genes were also affected in the DRG, including *Bdnf*, *Sst*, *Gal*, *Htr1a*, and *NmU*, which were down-regulated, and *Fkbp5*, *Htr4*, *Epha7*, and *Unc5d*, which were up-regulated (35, 36) (Fig. S5). qPCR of 26 robustly regulated and randomly selected genes showed a strong correlation with sequencing findings (Fig. 5*B*). The majority of DRG genes was not previously identified, and an overlay of our data with prior expression data for mouse cerebellum and hypothalamus (35, 36) reveals that 13% were identified previously, with the remainder unique to the rat DRG (Fig. 5*C*). There also appears to be limited overlap between our findings for the DRG and those reported for the hypothalamus of the MeCP2 KO rat (21), suggesting that differences may be tissue-specific.

Because MeCP2 is a master transcriptional regulator that influences (often subtly) expression of hundreds of genes, we reasoned that MeCP2's effects are likely to be a result of multiple gene interactions associated with specific defined biological pathways. Because altered spinal cord transmission at the level of the DRG central projection has been implicated in abnormal tactile sensitivity in a RTT mouse model (18), we assessed functional pathways associated with spinal sensory processing. Ingenuity pathway analysis (IPA) revealed significant modulation of canonical pathways associated with neurotransmission (Fig. 5*D*), including "neuropathic pain signaling in dorsal horn neurons" and "glutamate receptor signaling." However, both pathways were significantly down-regulated (4.5- and 1.7-fold, respectively). Similarly, of 32 expressed genes associated with GABA signaling in DRG neurons (Dataset S1), only two were regulated by MeCP2 disruption (*Gabra1* and *Gabra3*, +1.24- and −1.48-fold, respectively). Hence, these analyses did not provide strong evidence supporting the idea that altered central synaptic neurotransmission accounts for mechanical and cold hypersensitivity seen in the RTT rat.

We next explored those pathways that were identified by IPA as strongly regulated by MeCP2 inactivation. The most robustly up-regulated canonical pathway was "axonal guidance signaling," followed by pathways associated with cellular motility, calcium and second messenger signaling, and extracellular matrix regulation (Fig. 5*D*). Gene groupings according to pathway function also emphasized effects on motility, cell morphology, and signaling (Fig. S5). Given that signaling pathways seemed to be regulated, we performed a comprehensive examination of transient receptor potential (TRP) channels because of their substantial role in DRG sensory transduction. The only TRP genes showing significant up-regulation were TRPC5 (1.47-fold), which is a cold transducer (37), and TRPC4 (1.64-fold), which is implicated in axon regeneration and outgrowth (38). Significantly down-regulated genes were TRPM2 (−1.24-fold), an injury-associated Ca^{2+}channel (39), the principal cold sensor TRPM8

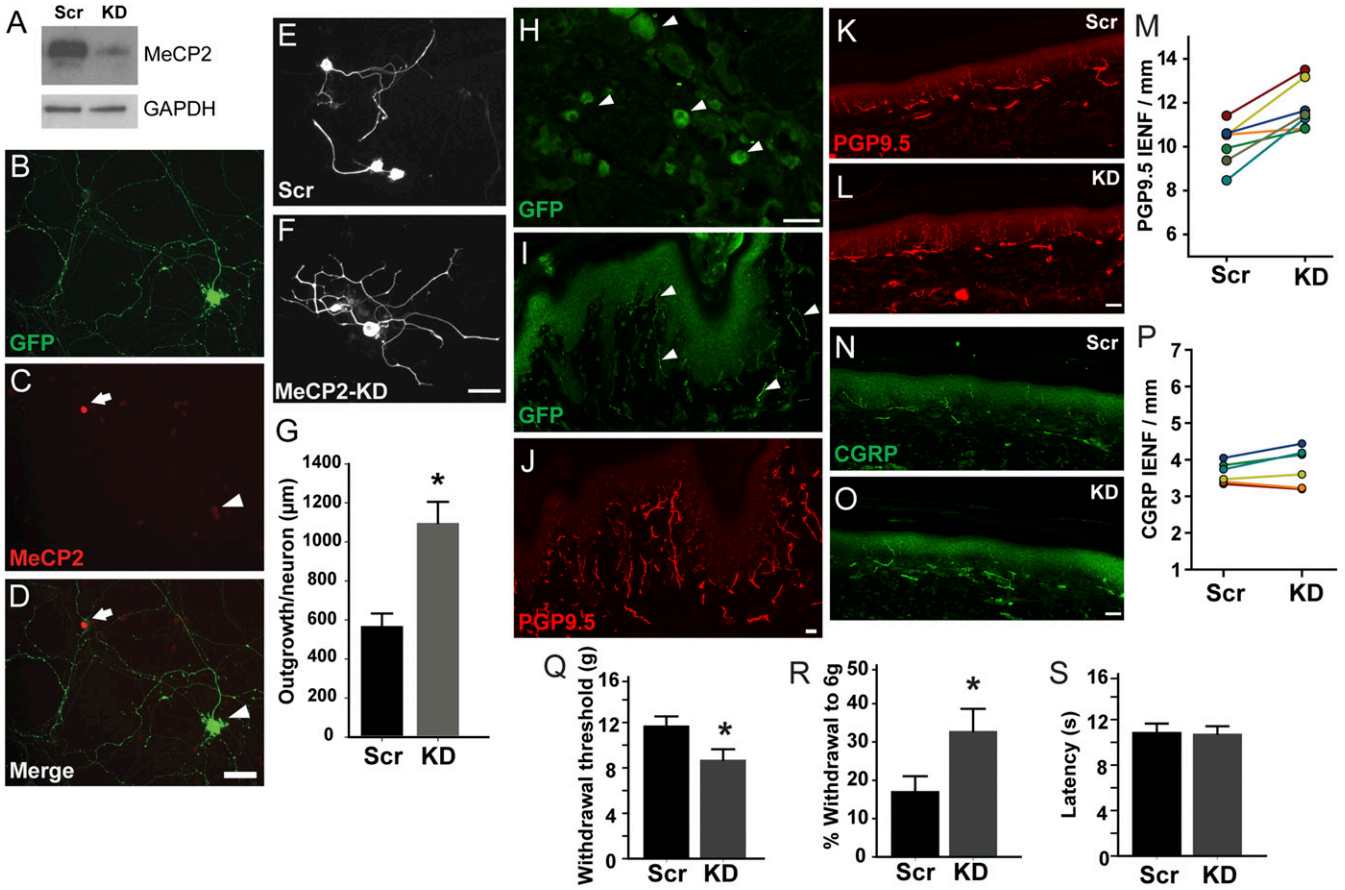

Fig. 4. MeCP2 knockdown in footpad-projecting DRG neurons induces hyperinnervation and hypersensitivity. (*A*) Western blot showing >80% knockdown efficiency of MeCP2 protein by lentiviral MeCP2 shRNA (KD) compared with scrambled shRNA sequence (Scr) in 50B11 cells, with GAPDH as a control. (*B*) GFP expression confirms viral transduction in a WT DRG neuron. MeCP2 staining is knocked down in transduced neuron (*C*, arrowhead) but not in an untransduced neuron (*D*, arrow). (*E*) DRG neurons receiving scrambled RNA (Control Scr) show typical neurites, whereas MeCP2 knockdown neurons show increased total neurite outgrowth (*F* and *G*, $*P = 0.02$, $n = 75$–100 neurons per group). (*H*–*J*) MeCP2 shRNA lentivirus engineered for efficient retrograde transport transduces footpad DRG neurons. (*H*) GFP expression in several L4 DRG neurons (arrowheads) confirms successful transduction 30 d following postnatal day 7 footpad injection of retrogradely transported lentiviral vector. (*I*) Footpad epidermal fibers also display GFP (arrowheads). (*J*) PGP9.5 staining of the section in *I* shows overall innervation. (*K*–*M*) MeCP2 knockdown induces nonpeptidergic hyperinnervation. (*K*) PGP9.5-ir innervation after injection of scrambled shRNA. (*L*) A footpad injected with MeCP2 shRNA shows more frequent PGP9.5-ir intraepidermal nerve fibers. (*M*) Numbers of PGP9.5-ir IENF are increased in knockdown footpads relative to the contralateral paw receiving scrambled shRNA ($*P = 0.012$, paired *t* test; $n = 6$). (*N*) CGRP immunostaining in the control footpad. (*O*) Fiber density of MeCP2 in KD paw appears comparable. (*P*) Comparison of CGRP IENFs between paws shows no significant difference (paired *t* test, $n = 6$). (*Q*–*S*) MeCP2 knockdown induces mechanical hypersensitivity. (*Q*) Mechanical sensitivity, as assessed by von Frey monofilaments (force in *g*), shows reduced threshold of footpads injected with MeCP2-knock down shRNA relative to scrambled RNA ($*P = 0.022$, $n = 6$). (*R*) The probability that a normally subthreshold stimulus elicits a response is also increased following MeCP2 knockdown ($*P = 0.037$, $n = 6$). (*S*) Withdrawal response latencies (in seconds) to footpad warming are comparable in paws receiving scrambled or knockdown shRNA ($n = 6$). (Scale bars, 50 μm.)

(40) (−1.28-fold), and TRPC3 (−1.44-fold), which is a mechanotransductive channel (41).

Pharmacological Down-Regulation of MeCP2 Target Long Genes Attenuates Abnormal Axon Outgrowth. Because MeCP2 preferentially regulates long (<100 kb) genes (42–44), we analyzed the functions and role of this subset of genes to provide additional insight into affected pathways. We confirmed that lengths of up-regulated genes were greater than those of down-regulated genes (43) (Fig. 6*A*), and genes longer than 100 kb also were up-regulated with greater frequency than those below 100 kb (Fig. 6*B*). To determine if long genes are functionally relevant to axon outgrowth, we cultured MeCP2 KO and WT DRG neurons for 48 h in different concentrations of topotecan (43), a topoisomerase inhibitor that selectivity blocks long gene transcription (42–44). Relative to WT cultures (Fig. 6*C*), KO neurons expectedly showed greater outgrowth (Fig. 6*D*). KO neuronal outgrowth was reduced dose-dependently by topotecan, whereas this agent had limited effect on WT axon outgrowth (Fig. 6 *E* and *F*). We also used qPCR to analyze a set of strongly regulated, growth-associated long genes in RNA from topotecan-treated DRG neuron cultures. Expression of these genes was uniformly reduced by low concentrations of topotecan to levels approximating those of WT neurons (Fig. 6*G*), whereas effects on WT neuronal gene expression were not apparent except at the highest concentration (Fig. S6).

Because topotecan prevented excessive sprouting characteristic of MeCP2-deficient neurons, we analyzed our gene set with regard to functional and canonical pathways most strongly affected by long gene suppression. Pathways were uniformly biased toward axon outgrowth and guidance, the plasma membrane, actin, and the cytoskeleton (Fig. S6). Thus, MeCP2 mutation preferentially up-regulates long genes that control neuritogenesis and related events involving cytoskeletal dynamics, and inhibition of these genes attenuates axonogenesis.

Selective Modulation of Key Affected Genes Prevents Abnormal Axonal Growth. Based on our dataset and analyses, several genes and gene families appear well positioned to play key roles in regulating

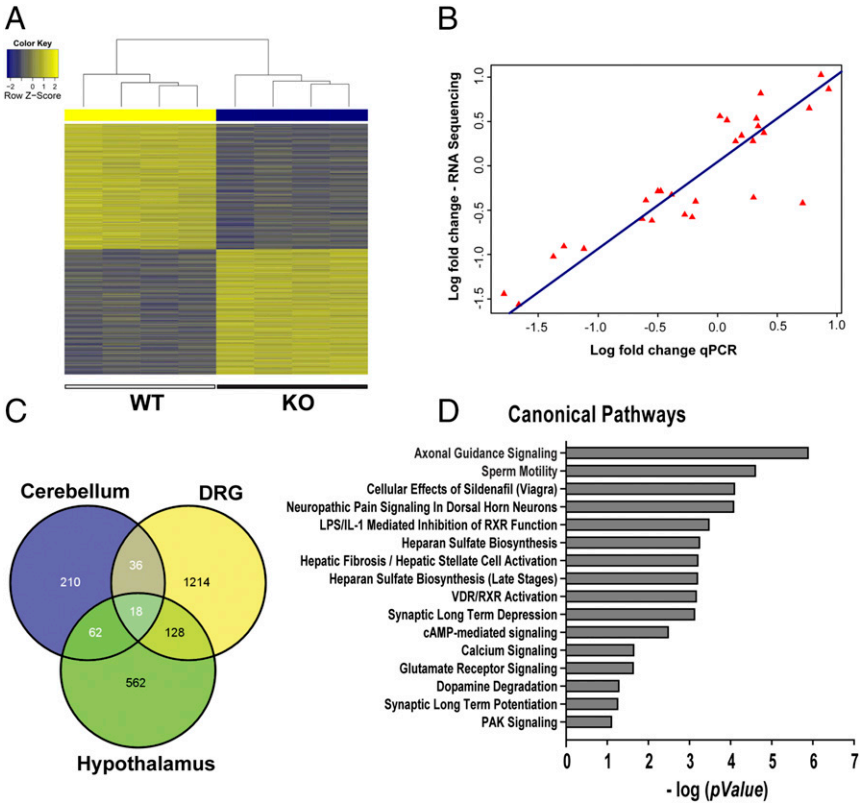

Fig. 5. MeCP2 KO selectively alters DRG genes regulating actin dynamics and neuritogenesis. (*A*) Heat map analysis of counts obtained from mapped reads shows that samples cluster by genotype. (*B*) Plot of RNA-Sequencing fold-changes vs. qPCR fold-changes of multiple candidate genes reveals a strong correlation ($r^2 = 0.89$, $P < 0.001$). (*C*) Comparison of number of differentially expressed genes in DRG with that reported in the literature for brain regions that also used ± 1.2 fold-change and 0.05 false-discovery rate (FDR) cut-off. (*D*) IPA identified major canonical pathways affected by MeCP2 disruption in sensory neurons (*x* axis = negative log to base 10).

cytoskeletal dynamics and axon outgrowth. In particular, the Arhgap (RhoGAP) family of genes, which encodes Rho GTPase-activating proteins, was up-regulated. Arhgaps catalyze hydrolysis of GTP by inactivating Rho, Rac, and Cdc42, thereby regulating actin polymerization necessary for axon outgrowth and other cytoskeletal functions (45). Arhgaps 10, 18, 19, 24, 28, 31, 36, and 42 were all up-regulated from 25 to 82%, with Arhgap36 showing the largest change. Up-regulation of these RhoGAPs is consistent with enhanced neuritogenesis because of augmented actin polymerization (46). In addition, RhoF, which restricts filopodia formation and is downstream to the Arhgaps, was down-regulated by 40% and would further promote axon growth (40). Similarly, Tiam1 and -2 regulate actin cytoskeleton in Rac-mediated axonogenesis (47, 48) and were up-regulated. qPCR confirmed MeCP2 regulation of these genes and revealed fold-changes consistent with those obtained by RNA-Seq (Fig. S5). Both Arhgap24 (Filgap) and protocadherin (PCdh)15 are up-regulated and are strongly implicated in providing structural contiguity among membrane channels, cytoskeletal tethers, and focal-adhesion anchor sites necessary for transduction of mechanical stimuli in filopodia and growth cone attachment (49–53). Collectively, these changes in gene expression suggest that a dominant effect of MeCP2 inactivation in DRG neurons is to alter actin polymerization, focal-adhesion formation, and other aspects of cytoskeletal dynamics associated with axon extension.

To identify regulated genes that may be playing key roles in abnormal axon outgrowth, we screened candidate genes for the ability to promote sensory neuritogenesis in the 50B11 rat DRG neuronal cell line (32, 33). In these cells, MeCP2 knockdown evoked a neuritogenic response similar to that seen in primary neurons (Fig. S7), confirming that MeCP2 regulates outgrowth in this cell line similar to that in primary DRG neuronal cultures, and validating this model as suitable for a high-throughput assay of candidate genes. Cells receiving lentiviral delivery of scrambled shRNA showed outgrowth similar to controls (Fig. S7). However, 50B11 cells receiving shRNA for Tiam1 and other candidate genes exhibited fewer and shorter neurites (Fig. S7), indicating critical roles of these genes in neuritogenesis. Similarly, the actin modulators Arhgap36 and Tiam1 were both effective in reducing neurite outgrowth. Knockdown of the focal-adhesion molecules cadherin (Cdh)11 and PCdh1 did not alter DRG neurite formation, whereas Cdh8 and PCdh15 knockdowns both reduced outgrowth (Fig. S7). Thus, many of the genes identified in our analyses do play key roles in axon outgrowth and would be expected to contribute to the sensory neuron phenotype in RTT.

Targeted Knockdown of Key Genes Regulating Actin Dynamics Abrogates RTT Neuroanatomical and Behavioral Phenotypes. If up-regulation of key genes controlling actin and associated cytoskeletal dynamics is responsible for sensory hyperinnervation and contributes to mechanical hypersensitivity, then down-regulating these genes in the MeCP2 KO rat should reverse this phenotype. Because of apparent redundancy in affected pathways, we selected eight genes showing robust up-regulation and playing key roles in promoting actin polymerization (Arhgaps 19, 24, 31, 36, and 42, and Tiam1) (54–56) and focal-adhesion formation (Cdh8 and PCdh15) (57). In preparatory experiments using 50B11 cell cultures, we confirmed that gene expression is significantly (>70–80%) suppressed by administering lentiviral shRNAs directed against these genes (Fig. S8). We then treated cultured DRG neurons from *Mecp2*$^{-/y}$ rats with the lentiviral shRNA "mixture" or with scrambled shRNA. Cultures receiving the scrambled control vectors showed vigorous axon outgrowth similar to that seen previously in MeCP2 KO DRG neurons. However, cultured neurons successfully transduced with the shRNA mix showed reduced axon outgrowth and down-regulation of the appropriate genes (Fig. S8), confirming that these genes play critical roles in axonogenesis in vitro.

We next injected the viral mixture subepidermally into the hind paw footpad of P7 *Mecp2*$^{-/y}$ rats, while the contralateral control footpad received virus containing scrambled shRNA. At 30 d, mechanical and thermal sensitivities were measured bilaterally. On the control side, mechanical hypersensitivity characteristic of MeCP2 KO was observed. However, mechanical sensitivity was reduced following administration of the knockdown mixture, as

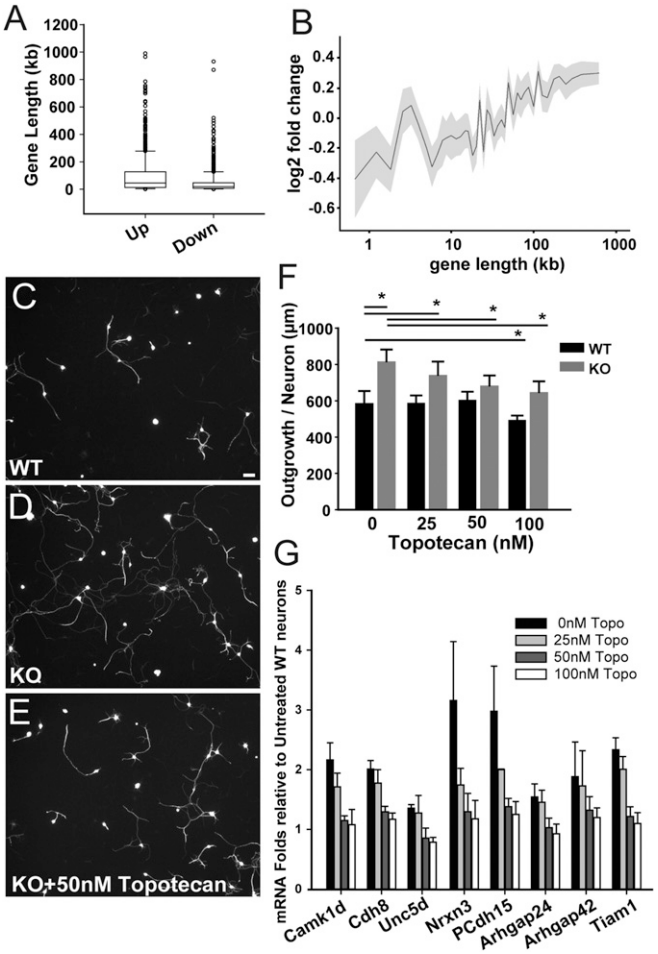

Fig. 6. MeCP2 knockout affects expression of long genes regulating actin cytoskeletal dynamics and neurite outgrowth. (*A*) Comparison of lengths of up- and down-regulated genes in *Mecp2*$^{-/y}$ sensory neurons (Mann–Whitney *u* test, $P < 0.001$). (*B*) Gene expression plotted as the binary log of fold-change with respect to the corresponding lengths of MeCP2-regulated gene candidates. (*C*) DRG neuronal culture from WT rat stained for tubulin βIII demonstrating the extent of neurite outgrowth. (Scale bar, 50 μm.) (*D*) DRG neuronal culture of a *Mecp2*$^{-/y}$ KO rat showing enhanced neurite outgrowth. (*E*) KO DRG neurons cultured in the presence of 50-nM topotecan treatment, showing reduction in neurite lengths. (*F*) Effects of topotecan treatment on neurite outgrowth by KO and WT primary sensory neurons. Topotecan was added to cultures at concentrations of 0, 25, 50, 100 nM (*$P < 0.001$, WT-0 vs. KO-0; $P < 0.001$, KO-0 vs. KO-50; $P < 0.001$, KO-0 vs. KO-100; $P = 0.03$, WT-0 vs. WT100. Two Way ANOVA, $n = 100$–300 neurons per group). (*G*) Effects of topotecan on selected long gene expression in KO primary neurons. KO neurons were cultured in different concentrations of topotecan and RNA fold-changes of candidate long genes compared with expression in WT.

evidenced by increased withdrawal threshold (Fig. 7*A*) and reduced responses to subthreshold stimulation (Fig. 7*B*). Thermal sensitivity was not significantly affected (Fig. 7*C*). Examination of the harvested footpads showed an overall reduction of PGP9.5-ir IENF density following viral knockdown (Fig. 7 *D*–*F*). CGRP-ir nerves were also reduced in skin (Fig. 7 *G*–*I*), but neither CGRP-ir nor IB4 innervation of the dorsal horn was affected (Fig. S4).

To confirm that the viral mixture effectively inhibited targeted gene expression, L3–L5 DRGs were enzymatically dissociated and GFP^{+} cells selected by flow cytometric sorting. qPCR of these samples revealed effective in vivo knockdown (~40–75% reduction) of the targeted genes (Fig. 7*J*). In contrast to KO rats, gene knockdown in WT rats did not alter innervation density or mechanical sensitivity (Fig. S9). Therefore, suppressing overexpressed key genes involved in actin dynamics and focal-adhesion formation is sufficient to restore innervation density and mechanical sensitivity of the MeCP2 KO rat toward the WT phenotypes.

Discussion

The primary findings of this study are that MeCP2 disruption leads to changes in DRG neuronal transcription that selectively target pathways involved in cytoskeletal dynamics, resulting in abnormal axon outgrowth and modality-specific changes in sensory behavior.

The finding of altered sensitivity in RTT rats is not altogether surprising, given prior reports concerning humans and animal models. Although abnormal sensitivity is reported in RTT, both hyper- and hyposensitivity have been noted (9–15); in this regard the observed modality-specific alterations in mechanical and thermal sensitivity may be especially relevant. There are a number of anecdotal reports of insensitivity, a classic one being a child who displayed insensitivity to open flame (58). In the RTT rat we observed thermal hyposensitivity and, consistent with this, reduced numbers of CGRP-ir peripheral and central fibers. One curious observation is that, whereas all identified neuronal subpopulations show increased outgrowth in culture with MeCP2 disruption, peptidergic axons were reduced centrally and peripherally in vivo, implying that extrinsic cellular interactions in this case may ultimately determine innervation density.

In contrast to heat insensitivity, cold and pressure sensitivity were elevated in RTT rats. Noxious cold transduction is mediated by members of the TRP family of receptor ion channels, notably TRPM8 (40) and to a lesser extent TRPC5 (37). Possibly consistent with increased cold sensitivity, TRPC5 showed up-regulation; however, TRPM8 was down-regulated, suggesting that cold hypersensitivity is not simply because of up-regulation of receptor genes and that other mechanisms must pertain. It is relevant that cold responsiveness is inhibited at the spinal level by peptidergic fibers (28); the decrease in dorsal horn peptidergic innervation noted in this study therefore may be a factor contributing to the augmented response to cold.

A prominent consequence of MeCP2 dysregulation is mechanical hypersensitivity. Pressure is detected primarily by epidermal free nerve endings of unmyelinated C and small myelinated A fibers projecting centrally to superficial layers of the dorsal horn. Conditional ablation studies show that the mechanical stimulation conducted in the present study is mediated primarily by nonpeptidergic small-diameter neurons (59), although it is not possible to exclude contributions from other fiber populations that may be affected by the MeCP2 mutation. Evidence from prior and current studies indicate that altered touch sensation is a result of the effects of MeCP2 disruption within the DRG itself. Orefice et al. (18), in a mouse model of RTT, found that abnormal tactile sensitivity, which is mediated by nonnociceptive low-threshold mechanosensitive DRG neurons, was replicated when an MeCP2 mutation was genetically restricted to the DRG. Our studies show that MeCP2 KD limited to the DRG is sufficient to induce mechanical hypersensitivity, which can be corrected by down-regulating key downstream genes. Hence, MeCP2-induced changes in DRG sensory neurons appear adequate to directly explain alterations in both tactile and nocifensive behaviors.

Why does MeCP2 disruption alter sensory function? Mouse studies suggest that anomalies of central connections may be responsible, as ganglion-specific MeCP2 KO results in loss of the majority of presynaptic inhibitory GABAergic signaling sites (18), which could lead to enhanced spinal excitatory neurotransmission. However, in the rat model, expression analysis of pathways and genes mediating GABAergic and glutaminergic transmission did not provide evidence of systematic changes that could reasonably account for enhanced mechanonosensitive behavior, and this was corroborated by the absence of changes in spinal cord nonpeptidergic innervation. Given that MeCP2-regulated genes show marked tissue- and species-specific variance, these results may not be surprising, and suggest that different

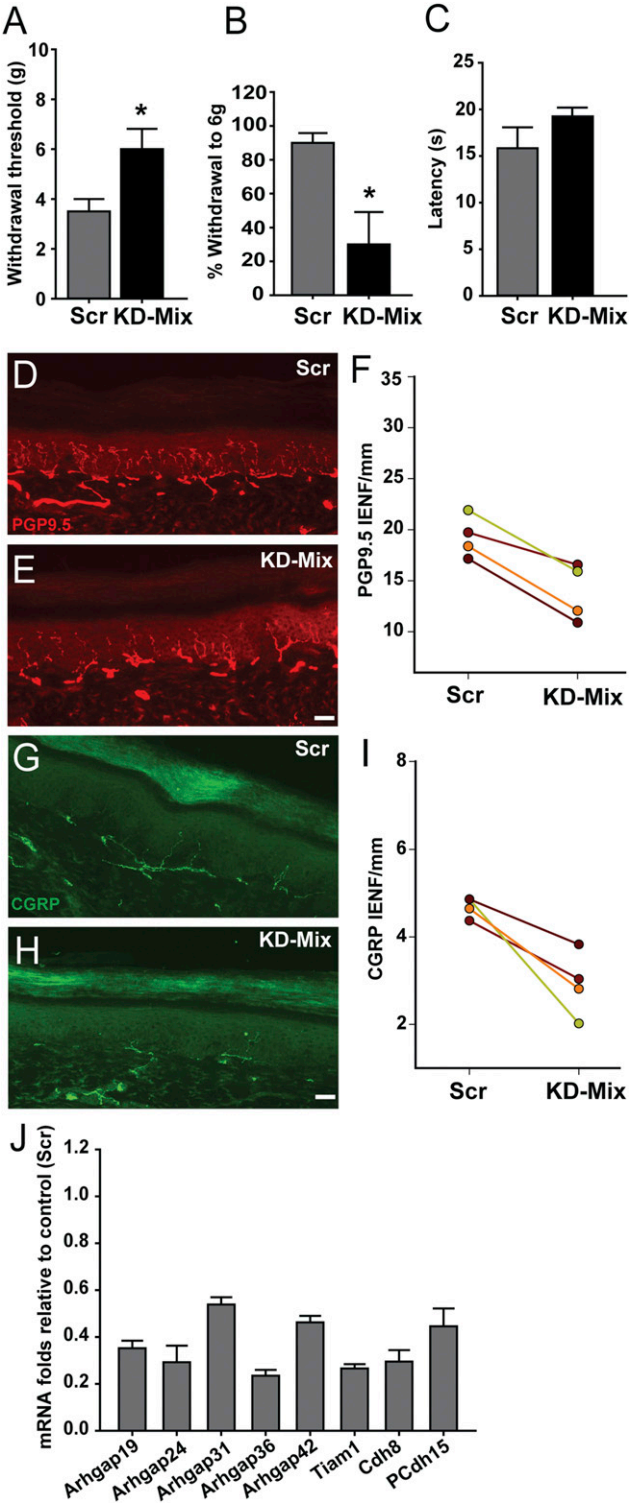

Fig. 7. Down-regulating key cytoskeleton-related genes normalizes neuroanatomical and behavioral phenotypes in *Mecp2*$^{-/y}$ rats. (*A*) Thirty days following lentiviral shRNA mixture injection (KD-Mix) into the hind paw, withdrawal threshold to mechanical stimulation was increased relative to scrambled shRNA control injection (*$P = 0.04$). (*B*) shRNA knockdown also reduced responsiveness to a subthreshold stimulus (*$P = 0.024$). (*C*) shRNA knockdown did not elicit a significant change in hind paw heat sensitivity ($P = 0.11$). (*D*) PGP9.5 labeling in scrambled-injected footpad shows innervation characteristic of *Mecp2*$^{-/y}$ KO rats. (*E*) PGP9.5-ir innervation appeared less after knockdown mixture injection. (*F*) Quantification confirmed reduced IENF per millimeter following knockdown mixture injection ($P = 0.006$). (*G*) Peptidergic innervation in *Mecp2*$^{-/y}$ footpad injected with scrambled shRNA revealed by CGRP immunostaining. (*H*) Peptidergic innervation appeared reduced following knockdown mixture-injected footpad. (*I*) Quantitation confirmed reduced peptidergic innervation after knockdown injection ($P = 0.021$). $n = 4$ *Mecp2*$^{-/y}$ rats in *A*, *B*, *C*, *F*, and *I*. (Scale bar, 50 μm.) (*J*) qPCR analysis of primary sensory neurons derived from footpad-injected rats and selected for GFP expression by FACS shows target gene down-regulation relative to scrambled transduced neurons ($n = 4$ samples each for scrambled and mixture).

sensory modalities can be altered by different mechanisms in RTT. Indeed, the contrasting effects on thermal and mechanical nocifensive pathways in RTT rat underscore this point.

Given that one of the most salient features of the rat RTT sensory phenotype is epidermal hyperinnervation, the role of changes in peripheral sensory terminals requires careful consideration. Increased numbers of cutaneous nonpeptidergic nerve endings in the RTT rat is strongly reminiscent of chronically painful conditions, such as vulvodynia (60), interstitial cystitis (61), myalgia (62), cancer (63), burns (64), and cutaneous inflammation (65), providing correlative data implicating nociceptor axon proliferation in hypersensitivity. Moreover, a functional link between inflammatory hyperalgesia and hyperinnervation has been noted, as blocking sensory angiotensin II type 2 receptors on sensory neurons concomitantly reduces hypersensitivity and axon numbers (65).

It is not clear how hyperinnervation might alter sensitivity. Some growing axons exhibit increased spontaneous activity (66) and highly branched axons tend to be more excitable (67), perhaps as a result of action potential summation or an expanded receptive field. More direct support for a causal relationship comes from current findings that suppressing the highly up-regulated gene pathways responsible for axonal actin polymerization and focal-adhesion formation reduces both peripheral innervation density and mechanical hypersensitivity. Actin polymerization and focal-adhesion formation are critical processes by which axons grow. Axon extension occurs through the Rho-dependent formation of filopodia that protrude from the axon by way of newly polymerized actin accumulating beneath the plasma membrane (53), and focal-adhesion sites that anchor them to the extracellular matrix (68).

Filopodia are critical for guiding growing axons, but are also mechanosensitive (53). The mechanisms by which filopodia of sprouting axons detect mechanical stimuli are not fully understood, but it is known that TRP receptors play critical roles (69). There is general agreement that these transmembrane proteins interact closely with cytoskeletal structures, which can act either as rigid elements transmitting stress to the membrane, which then deforms the channel and alters porosity (51), or as cellular tethers in which a channel's opening is initiated directly by force transmitted via a protein linker (70), such as Arhgap24 (49).

Our findings show that the MeCP2 mutation in DRG neurons leads to up-regulation of gene families that markedly affect dynamics of actin and other cytoskeletal components. This is likely to have two consequences. First, it would promote neurite outgrowth as predicted by IPA and confirmed by our observations of increased peripheral axon density. Second, it would be expected to "stiffen" cytoskeletal structures through which force is transmitted to cell membrane receptors, thus making them more responsive to pressure. Because our shRNA mixture delivered to footpad-projecting neurons would reduce both actin polymerization and focal adhesions, it would interrupt critical processes associated with axon growth and, presumably, actin cytoskeletal and adhesion proteins integral to mechanotransduction. Although the current experiments do not fully distinguish between the relative roles of axon sprouting and altered cytoskeletal transduction properties, they do reveal an obligatory role of actin and cytoskeletal dynamics in determining these features of the RTT sensory phenotype.

Methods

Behavior. All animal experiments were conducted on male rats and were approved by the University of Kansas Medical Center Institutional Animal Care and Use Committee. Associated protocols used in this study will be provided upon request. The MeCP2 KO rat was generated by a zinc finger nuclease mediated 71-bp deletion in exon 4 of *Mecp2* gene (product no. TGRA6090; Sage Labs). Mechanical sensitivity was analyzed using Siemens Weinstein monofilaments of known, graded force. Animals were placed in individual Plexiglas boxes on an elevated mesh table and allowed to acclimate for 20 min. Following acclimation, six monofilaments, ranging from 2 to 15 g, were applied five times to each hind paw at intervals of not less than 2 min. The number of positive responses, as observed by lifting or biting of the hind paw, was recorded. The calibrated force of the monofilament generating a 50% withdrawal response rate was recorded as the withdrawal threshold. Additionally, percentage withdrawal responses to a 6-g monofilament were determined.

Thermal sensitivity was measured as withdrawal latency to a fixed 4.85-A source directed to the paw in a Paw Thermal Stimulator (University of California, San Diego). The glass floor was maintained at 30.0 °C and 20 min of acclimation was allowed before testing. Light beam intensity was set at 4.85 A and withdrawal latency defined as the time from stimulus onset until the automatic sensor turned the light off in response to paw lifting. Thermal withdrawal latencies of each hind paw were measured in triplicate, with a minimum of 3 min between trials, and were averaged.

Cold sensitivity was measured using a Cold Plate Analgesia Meter (IITC). Rats were acclimated for 5 min at 25 °C, and thermal plate temperature was decreased at a ramp rate of 10 °C/min. On observing overt nociceptive behavior, such as lifting, biting, or licking of the hind paws, the thermal plate was immediately returned to 25 °C. Testing was conducted twice with a 5- to 10-min interval between trials. The average temperature at which nociceptive behaviors were seen is reported as the withdrawal threshold.

Cell Culture. T8-L6 DRGs were harvested bilaterally from 30- to 40-d rats, placed in ice-cold L15/3% glucose medium, chopped into three to four pieces, and incubated at 37 °C with 1 mg/mL collagenase (Sigma-Aldrich) and 2.5 U/mL dispase (Worthington) in HBSS for 40 min. Digestion was stopped by L15/10% FBS and cells were triturated, filtered through a 100-μm strainer, layered onto a 1.08 Percoll gradient column and centrifuged at 800 × *g* for 20 min. Pellets were washed in L15/glucose and plated on laminin/PDL-coated surfaces in Neurobasal A media (Life Technologies) containing glutamine, B27, and Primocin (InVivogen), as previously described (30).

The 50B11 cells were cultured on uncoated tissue culture plastic or glass surfaces in Neurobasal media (Life Technologies) containing B27, glucose, glutamine, 10% FBS, and Primocin (28). When confluent, cells were split and plated at 5,000–10,000 cells per well of a 24-well plate and after 24 h, differentiated by treatment with 75 μM forskolin. For outgrowth assays in gene knockdown experiments, cultures were fixed with 4% PFA 20–24 h after forskolin treatment (32).

Histology and Immunostaining. Rats were killed by isoflurane overdosage or intrapetitoneal injection of pentobarbital followed by decapitation or exsanguination. DRGs, footpads, dorsal hairy skin, brains, and spinal cords were harvested and fixed overnight at 4 °C in 4% paraformaldehyde (PFA) or Zamboni's fixative. In some cases, fresh tissue was postfixed in PFA after cryosectioning. Cell cultures were fixed for 20–30 min at room temperature in 4% paraformaldehyde. Cryo-sections were cut at 20 μm for the footpads and 10–14 μm for other tissues. Sections and cultures were blocked in 5% secondary host serum, 10% BSA, 0.3% Triton-X in PBS for 1 h and incubated overnight with primary antibodies and for 1 h for secondary antibodies.

Sections or cell cultures were immunostained for MeCP2 (rabbit monoclonal, 1:500–1,000; Cell Signaling Technology), PGP9.5 (rabbit IgG, 1:3,000; Serotec/Bio-Rad), CGRP (sheep IgG, 1:500; Biomol/Enzo), tubulin-βIII (mouse monoclonal, 1:500; Chemicon/Millipore), peripherin (chicken IgY, 1:400; Chemicon/Millipore), GFP (chicken IgY, 1:1,000; Aves), or stained with IB4–Alexa 488 conjugate (50 μg/mL; Life Technologies; with 1 mM $CaCl_2$ in PBS: 20-min staining). Secondary antibodies against rabbit, sheep, mouse, and chicken were generated in donkey or goat, conjugated to Cy3 (1:400; Jackson ImmunoResearch), Alexa 488, Alexa 555 (1:1,000; Life Technologies), or Dylight 488 (1:1,500; Jackson ImmunoResearch).

Imaging and Image Analysis. Images were acquired using Nikon TE300 and 80i fluorescence microscopes and a Nikon A1R confocal microscope. Images were analyzed using NIS-Elements, Metamorph, AnalySYS, and ImageJ with the NeuronJ Plugin. IENFs and neurite outgrowth were quantified as described previously (30, 62, 65).

Lentivirus. For MeCP2 knockdown studies, lentivirus was prepared using the pLKO1 or FG12 vector backbone. The 293T cells were plated overnight at 60–70% confluence and transfected with transfer vector, pMLDG-RRE, pRsv-Rev, pMD2.G using lipofectamine 2000. Virus-enriched supernatants were collected for up to 48 h and filtered and were used to transduce 50B11 cells or primary neuronal cultures. shRNAs used are listed in the Dataset S1.

For synthesis of lentiviral particles used for retrograde transport in footpad injections, the pMD2.G vector was replaced by the pFuGB2. Viral particles concentrated by ultracentrifugation were resuspended in sterile PBS and injected (1×10^5–10^6 particles in 8–10 μL) into the hind footpads of 7-d-old neonatal male rats. One foot was injected with shRNA against the target genes [i.e., MeCP2 shRNA for MeCP2 knockdown in experiments with WT pups, and shRNA mixture against Arhgaps 19, 24, 31, 36, and 42 (the five most up-regulated) (Dataset S1), Tiam1, Cdh8, and PCdh15 in the *Mecp2*$^{-/y}$ injection experiments] and the contralateral paw was injected with virus carrying scrambled shRNA control. The scrambled, MeCP2, Arghap36, and Tiam1 shRNAs were cloned from the pLKO1 into the FG12 vector backbone that expresses GFP to aid visual detection. The remaining shRNAs in the injection mixture were retained in the pLKO1 backbone. Injections were delivered using a 30-gauge needle attached to silicone tubing connected to a Hamilton syringe injection.

For lentiviral knockdown of seq-identified candidate genes in 50B11 cells and in primary neuons in vitro or in vivo, lentiviral shRNAs were delivered in the pLKO1 backbone and cells selected with puromycin; a scrambled shRNA was used for control and efficiency of knockdown tested by qPCR. The control and knockdown cells were differentiated for 24 h and outgrowth measured after staining (Vybrant CFDA SE Cell Tracer Kit; Life Technologies or PGP9.5).

PCR and Primers. RNA from T8–L6 DRGs was isolated by TRIzol and converted to cDNA using SuperScript II reverse transcriptase (Life Technologies). PCR was run on a Bio-Rad iCycler System using SYBR Green Master Mix (Bio-Rad). For FACS-sorted low-number GFP$^+$ neurons, the PicoPure RNA Isolation Kit (ARCTURUS; ThermoFisher) was used. Primers are listed in Dataset S1.

RNA Sequencing. RNA sequencing was performed on individual libraries generated from T8–L6 DRGs from four *Mecp2*$^{-/y}$ and four *Mecp2*$^{x/y}$ rats using an Illumina HiSeq2500 Sequencing System (Illumina) at the University of Kansas Medical Center Genomics Core. Total RNA (0.5 μg) was used to initiate the mRNA-Seq library preparation protocol. The mRNA fraction was enriched by oligo dT capture, sized, reverse-transcribed into cDNA, and ligated with the appropriate indexed adaptors using the TruSeq RNA Sample Preparation Kit v2 (RS-122–2001/2002; Illumina). Following Agilent Bioanalyzer QC of the library preparation and library quantification using a Roche Lightcycler96 with FastStart Essential DNA Green Master (Roche), the RNA-Seq libraries were adjusted to a 4-nM concentration and pooled for multiplexed sequencing. Libraries were denatured and diluted to the appropriate picomolar concentration (based on qPCR results) followed by clonal clustering onto the sequencing flow cell using the TruSeq Paired-End Cluster Kit v3-cBot-HS (Illumina). RNA-Sequencing was performed at a 2 × 50-bp paired-end resolution using the TruSeq SBS Kit v3-HS. The control and treatment samples were analyzed in biological quadruplicates, giving eight samples in total. Following collection, sequence data were converted from bcl file format to fastQ files and de-multiplexed into individual sequences for further downstream analysis. Reads were mapped to the rat genome (Rnor 5.0) using the STAR software, v2.3.1z (71), resulting in 34.4–49.2 million mapped reads per sample. Differential gene expression analysis was performed using Cuffdiff, v2.1.1 with additional analysis using EdgeR. The resulting *P* values were adjusted for multiple hypothesis testing. Biological and functional pathways of affected genes were assessed using IPA. Sequencing data are available at the Gene Expression Omnibus (accession no. GSE87855).

ACKNOWLEDGMENTS. We thank Dr. Ahmet Höke of the Johns Hopkins University for his gift of 50B11 cells; Drs. Anuradha Chakrabarty, Zhaohui Liao, and Sarah Tague for technical guidance; the staff of the Kansas Intellectual and Developmental Disabilities Research Center, particularly Jing Huang and Phil Shafer; and Drs. Julie A. Christianson, Kenneth McCarson, and Doug Wright for providing valuable input. Funding was provided by National Institute of Child Health and Human Development (NICHD) Grant R01HD049615, with core support from NICHD P30 HD002528 and U54 HD090216 and the University of Kansas Medical Center's Biomedical Research Training Program and Institute of Reproductive Health and Regenerative Medicine.

1. Zoghbi HY (2005) MeCP2 dysfunction in humans and mice. *J Child Neurol* 20:736–740.
2. Nomura Y, Segawa M (2005) Natural history of Rett syndrome. *J Child Neurol* 20: 764–768.
3. Amir RE, et al. (1999) Rett syndrome is caused by mutations in X-linked MECP2, encoding methyl-CpG-binding protein 2. *Nat Genet* 23:185–188.
4. Gonzales ML, LaSalle JM (2010) The role of MeCP2 in brain development and neurodevelopmental disorders. *Curr Psychiatry Rep* 12:127–134.
5. Belichenko PV, et al. (2009) Widespread changes in dendritic and axonal morphology in Mecp2-mutant mouse models of Rett syndrome: Evidence for disruption of neuronal networks. *J Comp Neurol* 514:240–258.
6. Wang IT, Reyes AR, Zhou Z (2013) Neuronal morphology in MeCP2 mouse models is intrinsically variable and depends on age, cell type, and Mecp2 mutation. *Neurobiol Dis* 58:3–12.
7. Xu X, Miller EC, Pozzo-Miller L (2014) Dendritic spine dysgenesis in Rett syndrome. *Front Neuroanat* 8:97.
8. Ricceri L, De Filippis B, Laviola G (2008) Mouse models of Rett syndrome: From behavioural phenotyping to preclinical evaluation of new therapeutic approaches. *Behav Pharmacol* 19:501–517.
9. Devarakonda KM, Lowthian D, Raghavendra T (2009) A case of Rett syndrome with reduced pain sensitivity. *Paediatr Anaesth* 19:625–627.
10. Downs J, et al. (2010) Linking MECP2 and pain sensitivity: The example of Rett syndrome. *Am J Med Genet A* 152A:1197–1205.
11. Konen AA, Joshi GP, Kelly CK (1999) Epidural analgesia for pain relief after scoliosis surgery in a patient with Rett's syndrome. *Anesth Analg* 89:451–452.
12. O'Leary HM, et al. (2017) Detecting autonomic response to pain in Rett syndrome. *Dev Neurorehabil* 20:108–114.
13. Barney CC, Feyma T, Beisang A, Symons FJ (2015) Pain experience and expression in Rett syndrome: Subjective and objective measurement approaches. *J Dev Phys Disabil* 27:417–429.
14. Cianfaglione R, et al. (2015) A national survey of Rett syndrome: Age, clinical characteristics, current abilities, and health. *Am J Med Genet A* 167:1493–1500.
15. Symons FJ, Byiers B, Tervo RC, Beisang A (2013) Parent-reported pain in Rett syndrome. *Clin J Pain* 29:744–746.
16. Symons FJ, et al. (2008) Evidence of altered epidermal nerve fiber morphology in adults with self-injurious behavior and neurodevelopmental disorders. *Pain* 134: 232–237.
17. Symons FJ, et al. (2015) Peripheral innervation in children with global developmental delay: Biomarker for risk for self-injurious behavior? *J Child Neurol* 30:1722–1727.
18. Orefice LL, et al. (2016) Peripheral mechanosensory neuron dysfunction underlies tactile and behavioral deficits in mouse models of ASDs. *Cell* 166:299–313.
19. Mogil JS (2009) Animal models of pain: Progress and challenges. *Nat Rev Neurosci* 10: 283–294.
20. Wu Y, et al. (2016) Characterization of Rett syndrome-like phenotypes in Mecp2-knockout rats. *J Neurodev Disord* 8:23.
21. Patterson KC, Hawkins VE, Arps KM, Mulkey DK, Olsen ML (2016) MeCP2 deficiency results in robust Rett-like behavioural and motor deficits in male and female rats. *Hum Mol Genet* 25:3303–3320.
22. Veeraragavan S, et al. (2016) Loss of MeCP2 in the rat models regression, impaired sociability and transcriptional deficits of Rett syndrome. *Hum Mol Genet* 25:3284–3302.
23. Skene PJ, et al. (2010) Neuronal MeCP2 is expressed at near histone-octamer levels and globally alters the chromatin state. *Mol Cell* 37:457–468.
24. Kaufmann WE, Johnston MV, Blue ME (2005) MeCP2 expression and function during brain development: Implications for Rett syndrome's pathogenesis and clinical evolution. *Brain Dev* 27(Suppl 1):S77–S87.
25. Manners MT, Ertel A, Tian Y, Ajit SK (2016) Genome-wide redistribution of MeCP2 in dorsal root ganglia after peripheral nerve injury. *Epigenetics Chromatin* 9:23.
26. Tochiki KK, Cunningham J, Hunt SP, Géranton SM (2012) The expression of spinal methyl-CpG-binding protein 2, DNA methyltransferases and histone deacetylases is modulated in persistent pain states. *Mol Pain* 8:14.
27. Cohen S, et al. (2011) Genome-wide activity-dependent MeCP2 phosphorylation regulates nervous system development and function. *Neuron* 72:72–85.
28. McCoy ES, et al. (2013) Peptidergic CGRPα primary sensory neurons encode heat and itch and tonically suppress sensitivity to cold. *Neuron* 78:138–151.
29. Zylka MJ (2005) Nonpeptidergic circuits feel your pain. *Neuron* 47:771–772.
30. Bhattacherjee A, Rumi MA, Staecker H, Smith PG (2013) Bone morphogenetic protein 4 mediates estrogen-regulated sensory axon plasticity in the adult female reproductive tract. *J Neurosci* 33:1050–1061a.
31. Ferri GL, et al. (1990) Neuronal intermediate filaments in rat dorsal root ganglia: Differential distribution of peripherin and neurofilament protein immunoreactivity and effect of capsaicin. *Brain Res* 515:331–335.
32. Bhattacherjee A, Liao Z, Smith PG (2014) Trophic factor and hormonal regulation of neurite outgrowth in sensory neuron-like 50B11 cells. *Neurosci Lett* 558:120–125.
33. Chen W, Mi R, Haughey N, Oz M, Höke A (2007) Immortalization and characterization of a nociceptive dorsal root ganglion sensory neuronal line. *J Peripher Nerv Syst* 12: 121–130.
34. Kato S, et al. (2011) Selective neural pathway targeting reveals key roles of thalamostriatal projection in the control of visual discrimination. *J Neurosci* 31:17169–17179.
35. Ben-Shachar S, Chahrour M, Thaller C, Shaw CA, Zoghbi HY (2009) Mouse models of MeCP2 disorders share gene expression changes in the cerebellum and hypothalamus. *Hum Mol Genet* 18:2431–2442.
36. Chahrour M, et al. (2008) MeCP2, a key contributor to neurological disease, activates and represses transcription. *Science* 320:1224–1229.
37. Zimmermann K, et al. (2011) Transient receptor potential cation channel, subfamily C, member 5 (TRPC5) is a cold-transducer in the peripheral nervous system. *Proc Natl Acad Sci USA* 108:18114–18119.
38. Wu D, Huang W, Richardson PM, Priestley JV, Liu M (2008) TRPC4 in rat dorsal root ganglion neurons is increased after nerve injury and is necessary for neurite outgrowth. *J Biol Chem* 283:416–426.
39. Naziroğlu M, et al. (2013) Role of TRPM2 cation channels in dorsal root ganglion of rats after experimental spinal cord injury. *Muscle Nerve* 48:945–950.
40. Bautista DM, et al. (2007) The menthol receptor TRPM8 is the principal detector of environmental cold. *Nature* 448:204–208.
41. Quick K, et al. (2012) TRPC3 and TRPC6 are essential for normal mechanotransduction in subsets of sensory neurons and cochlear hair cells. *Open Biol* 2:120068.
42. King IF, et al. (2013) Topoisomerases facilitate transcription of long genes linked to autism. *Nature* 501:58–62.
43. Gabel HW, et al. (2015) Disruption of DNA-methylation-dependent long gene repression in Rett syndrome. *Nature* 522:89–93.
44. Sugino K, et al. (2014) Cell-type-specific repression by methyl-CpG-binding protein 2 is biased toward long genes. *J Neurosci* 34:12877–12883.
45. Govek EE, Newey SE, Van Aelst L (2005) The role of the Rho GTPases in neuronal development. *Genes Dev* 19:1–49.
46. Hall A, Lalli G (2010) Rho and Ras GTPases in axon growth, guidance, and branching. *Cold Spring Harb Perspect Biol* 2:a001818.
47. Kunda P, Paglini G, Quiroga S, Kosik K, Caceres A (2001) Evidence for the involvement of Tiam1 in axon formation. *J Neurosci* 21:2361–2372.
48. Tolias KF, et al. (2005) The Rac1-GEF Tiam1 couples the NMDA receptor to the activity-dependent development of dendritic arbors and spines. *Neuron* 45:525–538.
49. Ehrlicher AJ, Nakamura F, Hartwig JH, Weitz DA, Stossel TP (2011) Mechanical strain in actin networks regulates FilGAP and integrin binding to filamin A. *Nature* 478: 260–263.
50. Marshall KL, Lumpkin EA (2012) The molecular basis of mechanosensory transduction. *Adv Exp Med Biol* 739:142–155.
51. Ingber DE (2006) Cellular mechanotransduction: Putting all the pieces together again. *FASEB J* 20:811–827.
52. Hu J, Chiang LY, Koch M, Lewin GR (2010) Evidence for a protein tether involved in somatic touch. *EMBO J* 29:855–867.
53. Heckman CA, Plummer HK, 3rd (2013) Filopodia as sensors. *Cell Signal* 25:2298–2311.
54. Ehler E, van Leeuwen F, Collard JG, Salinas PC (1997) Expression of Tiam-1 in the developing brain suggests a role for the Tiam-1-Rac signaling pathway in cell migration and neurite outgrowth. *Mol Cell Neurosci* 9:1–12.
55. Lavelin I, Geiger B (2005) Characterization of a novel GTPase-activating protein associated with focal adhesions and the actin cytoskeleton. *J Biol Chem* 280:7178–7185.
56. Peck J, Douglas G, 4th, Wu CH, Burbelo PD (2002) Human RhoGAP domain-containing proteins: Structure, function and evolutionary relationships. *FEBS Lett* 528:27–34.
57. Leckband DE, de Rooij J (2014) Cadherin adhesion and mechanotransduction. *Annu Rev Cell Dev Biol* 30:291–315.
58. Hagberg B (2002) Clinical manifestations and stages of Rett syndrome. *Ment Retard Dev Disabil Res Rev* 8:61–65.
59. Cavanaugh DJ, et al. (2009) Distinct subsets of unmyelinated primary sensory fibers mediate behavioral responses to noxious thermal and mechanical stimuli. *Proc Natl Acad Sci USA* 106:9075–9080, and erratum (2009) 106:11424.
60. Bohm-Starke N, Hilliges M, Falconer C, Rylander E (1998) Increased intraepithelial innervation in women with vulvar vestibulitis syndrome. *Gynecol Obstet Invest* 46: 256–260.
61. Regauer S, Gamper M, Fehr MK, Viereck V (2017) Sensory hyperinnervation distinguishes bladder pain syndrome/interstitial cystitis from overactive bladder syndrome. *J Urol* 197:159–166.
62. Tague SE, et al. (2011) Vitamin D deficiency promotes skeletal muscle hypersensitivity and sensory hyperinnervation. *J Neurosci* 31:13728–13738.
63. Jimenez-Andrade JM, et al. (2010) Pathological sprouting of adult nociceptors in chronic prostate cancer-induced bone pain. *J Neurosci* 30:14649–14656.
64. Hamed K, et al. (2011) Changes in cutaneous innervation in patients with chronic pain after burns. *Burns* 37:631–637.
65. Chakrabarty A, Liao Z, Smith PG (2013) Angiotensin II receptor type 2 activation is required for cutaneous sensory hyperinnervation and hypersensitivity in a rat hind paw model of inflammatory pain. *J Pain* 14:1053–1065.
66. Jiang M, et al. (2013) Dendritic arborization and spine dynamics are abnormal in the mouse model of MECP2 duplication syndrome. *J Neurosci* 33:19518–19533.
67. Janse C, Peretz B, van der Roest M, Dubelaar EJ (1999) Excitability and branching of neuroendocrine cells during reproductive senescence. *Neurobiol Aging* 20:675–683.
68. Geiger B, Bershadsky A (2001) Assembly and mechanosensory function of focal contacts. *Curr Opin Cell Biol* 13:584–592.
69. Li Y, et al. (2005) Essential role of TRPC channels in the guidance of nerve growth cones by brain-derived neurotrophic factor. *Nature* 434:894–898.
70. Kung C (2005) A possible unifying principle for mechanosensation. *Nature* 436:647–654.
71. Dobin A, et al. (2013) STAR: Ultrafast universal RNA-seq aligner. *Bioinformatics* 29: 15–21.